

reasoning only applies when the distribution is of such a form that the Hankel transformed function has an infinite radius of convergence. As neither the cascade angular or radial distributions satisfy this criterion, we find that *there is no reason to believe that a knowledge of their moments can ever yield the behavior of the distributions at small values of the variables.*

The calculations we have performed of the track-length angular and radial distributions of the electron-photon cascade under the Landau approximation indicate that the Mellin transform method of reconstructing a function from its moments can be used for the evaluation of these distributions for all values of the angular variable $E\theta/E_s$ greater than 0.5 and of the radial variable Er/E_s greater than about 3. As this is a very simple calculation, it indicates that any future direct

evaluation of the angular or radial distribution functions need only be carried out for smaller values of the variables; at the larger values the functions are much more easily obtained from their moments. However, it must be pointed out that these estimates were made using values of the moments calculated under the Landau approximation. The increase in the higher moments that will ensue when this approximation is dropped will increase the minimum angle or radius at which the distribution can be obtained from its moments. The actual magnitude of this increase cannot as yet be estimated.

The author wishes to thank Professor H. Messel and Dr. J. M. Blatt for helpful discussions. He is also indebted to the Commonwealth Scientific and Industrial Research Organization for the provision of a research grant.

PHYSICAL REVIEW

VOLUME 105, NUMBER 2

JANUARY 15, 1957

Charged-Pion Production in Lithium†*

EDWIN K. GATCHELL‡

Department of Physics, University of Rochester, Rochester, New York

(Received March 12, 1956; revised version received October 24, 1956)

This article reports the measurement of charged-pion production cross sections in Li^6 and Li^7 . The measurements were made on 40- and 52-Mev pions emitted at 90° to a proton beam of 242-Mev energy. The results show a higher π^+/π^- ratio for Li^6 than for Li^7 ; this observation can be qualitatively explained by the Pauli exclusion principle.

I. INTRODUCTION

WE have measured the absolute cross sections for the production of charged pions by 242-Mev protons on Li^6 and Li^7 . The pions were emitted at 90° to the proton beam and measurements were made at pion energies of 40 and 52 Mev in the laboratory system.

The charge-independence prediction¹ for the production of pions by protons on nuclei of isotopic spin 0 is given by the Watson relation

$$2\sigma_0 = \sigma_+ + \sigma_-$$

where σ_0 is the differential production cross section for neutral pions, and σ_+ and σ_- are the corresponding differential cross sections for positive and negative pions. Since this experiment determines $\sigma_+ + \sigma_-$, a measurement of σ_0 at the same proton energy would constitute a test of the charge independence hypothesis.

† This research was assisted by the U. S. Atomic Energy Commission.

* Based on a thesis submitted to the Graduate School of the University of Rochester in partial fulfillment of the requirements for the degree of Doctor of Philosophy.

‡ Now at RCA Laboratories, Princeton, New Jersey.

¹ K. M. Watson, Phys. Rev. **85**, 852 (1952); A. M. L. Messiah, Phys. Rev. **86**, 430 (1952); J. M. Luttinger, Phys. Rev. **86**, 581 (1952).

This prediction assumes, however, that equivalent final nucleon states are available for each of the three modes of meson production. At proton energies not greatly in excess of threshold, the details of nuclear structure may obscure the charge-independence prediction. This experiment was undertaken to obtain new data on pion production in low- Z materials and to explore the utility of the Watson relation as a test of charge independence at the energies available with the Rochester synchrocyclotron.

II. EXPERIMENTAL ARRANGEMENT

The internal proton beam bombarded a 3 in. \times $\frac{3}{16}$ in. \times $\frac{1}{8}$ in. Li target located at a radius of 59 in. in the synchrocyclotron. Pions emitted in the median plane at 90° to the proton beam followed curved trajectories in the fringing field of the cyclotron. Floating-wire measurements were used to design a channel that defined the solid angle and energy interval of the emitted pions. The pions were detected in a scintillation crystal telescope by using pulse-height analysis to separate the pions from the background. The proton beam was measured absolutely using the $\text{C}^{12}(p,pn)\text{C}^{11}$ reaction from the carbon in a 2-mil polyethylene foil attached to the target.

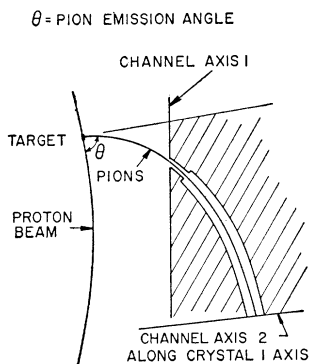


FIG. 1. Geometry for the 52-Mev channel.

III. PROCEDURE

A. Solid Angle and Energy Interval

The solid angle defined by a small rectangular crystal is $\Delta\Omega = \Delta\phi\Delta\theta$, where $\Delta\theta$ is the plane angle in the horizontal plane and $\Delta\phi$ is the angle in the vertical plane. Consider the horizontal plane first. The paths of trajectories in the median plane were mapped by the floating-wire technique. A rod simulating the target was mounted in bronze bearings so that it was free to rotate. The wire from the center of the rod, simulating the pion trajectory, then passed over a pulley and was loaded with a mass of 500 g. The current was then adjusted so that the wire corresponded to a given pion energy. The angle of emission of the wire with respect to a radius through the center of the target was measured by reflecting a cross hair from a mirror mounted on the rod in the same manner that galvanometer deflections are measured. Five or six trajectories separated by approximately 2° in horizontal emission angle were taken in the neighborhood of 90° at 35, 40, 45, 50, 55, and 60 Mev.

By using these trajectories, channels at 40 and 52 Mev were designed and analyzed. Figure 1 shows the geometry of the channel for 52-Mev pions where the emission angle in the horizontal plane is defined by the channel entrance and a $\frac{3}{8}$ -in. square scintillation crystal along axis (2). By plotting the intersection of trajectories of one energy with channel axis (1) or (2) as a function of horizontal emission angle, one can predict

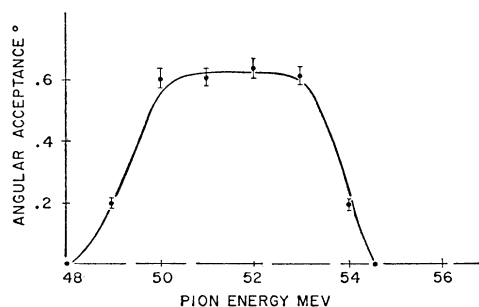


FIG. 2. Horizontal acceptance angle as a function of pion energy for 52-Mev pion channel.

the horizontal emission angle, $\Delta\phi$, subtended by the channel and scintillation crystal combination. Figure 2 shows the result of the analysis for the 52-Mev channel. The area under the curve then is $\Delta\theta\Delta E$. Since the target is $\frac{3}{16}$ in. thick and the above procedure assumes a point source, the analysis was repeated with the trajectories displaced $\frac{3}{32}$ in. on either side of the target position. The result is that $\Delta\theta\Delta E$ changes by less than 8% while the mean energy of the accepted pions changes by 1.3 Mev.

For small vertical displacements from the median plane, it can be shown that

$$\frac{d^2z}{ds^2} = -\frac{e}{pc} \frac{\partial H_z}{\partial s} \sin b,$$

where z = vertical displacement of pion from median plane, b = angle between radius vector from the center of the machine and the velocity vector of the pion, H_z = vertical component of magnetic field, and s = path length of pion from target. The function $\frac{\partial H_z}{\partial r}$ has

TABLE I. Energy interval for Li^6 and Li^7 targets—error in standard deviations.

Target energy	$\Delta\Omega\Delta E$ (sterad Mev)
Li^6 40 Mev	$(1.25 \pm 0.06) \times 10^{-3}$
Li^6 52 Mev	$(1.40 \pm 0.07) \times 10^{-3}$
Li^7 40 Mev	$(1.21 \pm 0.06) \times 10^{-3}$
Li^7 52 Mev	$(1.38 \pm 0.07) \times 10^{-3}$

recently been measured to better than 0.5%. $\sin b$ was measured from the trajectories and the equation was integrated numerically. The $\frac{3}{8}$ -in. \times $\frac{3}{8}$ -in. crystal, along channel axis (2), defined the beam vertically. From the numerical solutions, it was possible to determine $\Delta\phi$, the vertical angle subtended by the defining crystal, for any point along the target. The vertical proton distribution over the target, measured by cutting the polyethylene foil into strips and measuring the activity, was folded in with $\Delta\phi$ to give $\langle\Delta\phi\rangle_{Av}$, the mean vertical angle.

The largest error in the solid-angle—energy interval, $\langle\Delta\phi\rangle_{Av}\Delta\theta\Delta E$, is in $\Delta\theta$ which results from the error in emission angle of the wire of 0.1° giving a 5% error in $\Delta\theta$. Since the Li^6 target was $2\frac{1}{4}$ in. long and the Li^7 target was 3 in. long, there is a small difference between $\langle\Delta\phi\rangle_{Av}$ for the two cases due to the difference in proton distribution. Table I lists the results for Li^6 and Li^7 targets at 40 and 52 Mev.

B. Proton Beam

As an absolute beam intensity standard we used the $\text{C}^{12}(p, p^+)\text{C}^{11}$ reaction and counted positrons from a 2-mil polyethylene foil attached to the target. The counting was done with an end-window Geiger tube placed inside a Lucite-lined lead shield. The target foil

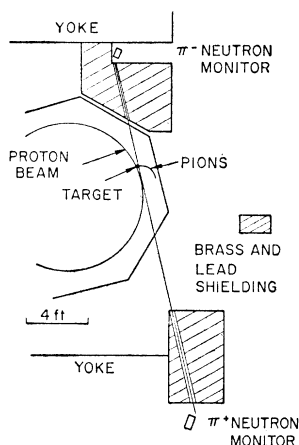
² E. M. Hafner (private communication).

was 20 cm below the counter so that the counting efficiency was constant over the 3-in. target length. This counting arrangement had been previously calibrated³ by using a radium D-E source from the Bureau of Standards for measuring $p-p$ and $p-d$ cross sections. Since that time Crandall *et al.*⁴ have remeasured the $C^{12}(p,pn)C^{11}$ cross section at 240 Mev and the agreement between Berkeley and Rochester $p-p$ cross sections is closer than the error quoted in either experiment. This development gives one considerable confidence in using this technique for absolute beam measurement.

The counter was equipped with a univibrator which reduced the counter voltage below threshold after each pulse thereby introducing a fixed dead time. All counting was done at rates such that the dead-time correction was less than 10%. The activity was followed for 4 half-lives and no other activity than the 20.5-min C^{11} half-life was ever observed.

In order to take pion production data, it was necessary to have a monitor and, for this purpose, two

Fig. 3. Shielding plan for neutron monitors.



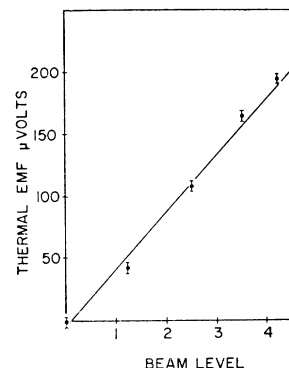
separate neutron-monitor telescopes were used as shown in Fig. 3. The axes of the telescopes were set at about 20° to the forward neutron beam and detected scattered protons from a block of paraffin placed at the entrance of the channel. Each telescope consisted of two Sintilon crystals separated by 3 in.

Since the proton beam was reversed to obtain both plus and minus pions, it was convenient to have some method of intercalibrating the two neutron monitors. This was accomplished by using a thermocouple to measure the heat flow from the target. Constantan wires were soldered at either end of the copper rod supporting the target. The thermal emf developed across the two constantan leads was measured by a Leeds and Northrup slide wire potentiometer. Since the heat flow down the rod is proportional to energy loss in the target, the

³ R. Schamberger, University of Rochester thesis, 1954 (unpublished); D. Klein, University of Rochester thesis, 1954 (unpublished).

⁴ Crandall, Millburn, Pyle, and Birnbaum, Phys. Rev. **101**, 329 (1956).

Fig. 4. Thermal emf vs beam level.



thermal emf is proportional to the proton beam. Figure 4 shows the linearity between the neutron monitor counts/min and the thermal emf. The thermal emf served as a check on the stability of the neutron monitors as well as a means of intercalibration. No significant drifts were found.

After the pion data were taken, the activity in the polyethylene foil was allowed to die out. A short calibration run was then made, the neutron-monitor counts recorded, and the foil beta counted. Upon using a value of 37.2 mb for the $C^{12}(p,pn)C^{11}$ reaction, the number of protons per neutron monitor was calculated. Then, by means of the thermal emf data, the other neutron monitor readings could be expressed in terms of protons.

C. Energy of the Proton Beam

Since pion production cross section is a sharp function of the proton energy, meaningful results require that the proton energy be carefully monitored. Radial oscillations produce an energy spread in the primary beam striking a fixed target and changes in radial oscillations cause variations in the mean energy of the proton beam. The energy of a proton is, for all practical purposes, equal to the synchronous orbit energy. However, a radial oscillation may cause a proton to strike the target at 59 in. with a synchronous orbit radius less than 59 in. and the proton energy would then be less than the synchronous orbit energy of 59 in.

Now the synchronous orbit energy and frequency of

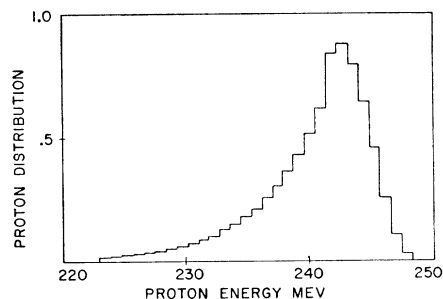


Fig. 5. Proton energy distribution.

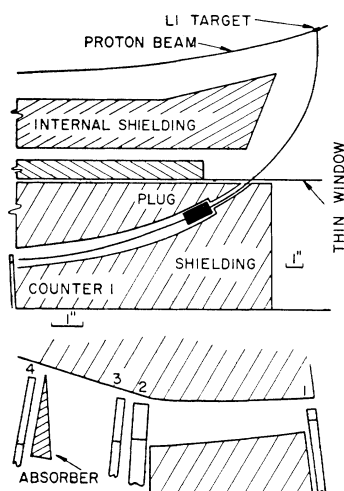


FIG. 6. Geometry of the 40-Mev pion channel.

revolution of the proton are related to the synchronous orbit radius $H(r)$ by

$$E = \frac{H(r)ec}{2\pi f(r)},$$

where E is the total energy of the proton. Since $H(r)$ is known for the Rochester machine, one obtains "D" voltage frequency as a function of the proton energy. For each prompt event such as a fast neutron or a meson, one needs only to measure the instantaneous frequency of the synchrocyclotron oscillator to determine the energy of the proton causing the event. This was accomplished by displaying the prompt pulses on a scope whose horizontal sweep was calibrated in terms of the frequency of the synchrocyclotron oscillator. The operating parameters of the cyclotron were adjusted to give the highest mean energy of the beam and the proton energy distributions were monitored continuously while final data on pion production were taken.

While the above method measures the effect of radial oscillations, it does not take recirculation into account. Clark⁵ has measured recirculation in the Rochester machine as a function of the multiple scattering in the target. By using his results, the effect

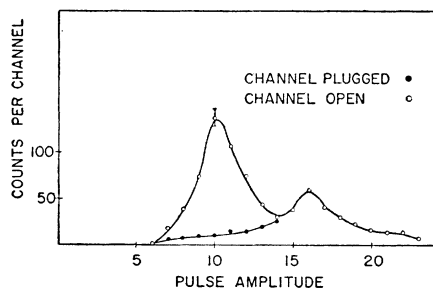


FIG. 7. Pion pulse-height distributions.

⁵ D. L. Clark, University of Rochester thesis, 1952 (unpublished).

of recirculation was calculated for the Li target and the effect of recirculation was folded into the distribution due to radial oscillations. The final distribution is shown in Fig. 5.

Pion Detection

Figure 6 shows the geometry of the pion channel and the scintillation telescope for the 40-Mev case. The geometry is such that the channel entrance and counter (1) define the beam. The distance between the (1) counter and the (2) counter represents a compromise between low signal-to-noise ratio when this distance is small and large multiple-scattering losses and inaccuracy in determining the solid-angle—energy interval when the one two distance is large.

In order to separate out the pions from the large background (caused by neutron-induced events), pulse height analysis is extremely useful. The electronics for this were straightforward. A fourfold coincidence with 5×10^{-8} -sec resolving time opened a 0.1- μ sec gate of a gated amplifier and the signal causing the coincidence

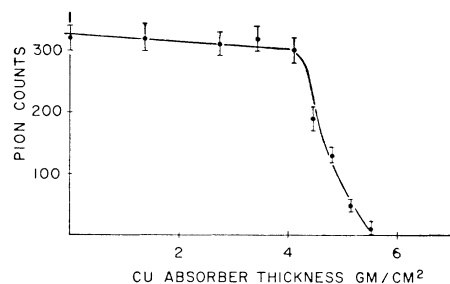


FIG. 8. Pion range curve for 40-Mev pions.

from counter two, appropriately centered in the gate, was fed into the input of the gated amplifier. The output of the amplifier fed a 24-channel pulse-height analyzer.

The counters were calibrated in a 50-Mev pion beam, deflected and focused with a wedge magnet into a well shielded auxiliary channel. Delay curves and voltage plateaus were taken and the pulse-height analyzer calibrated. Since 1-meter light pipes were necessary in order to shield the phototubes, high collection efficiency in the phototubes was necessary. For this reason relatively slow DuMont 6292 and 6291 phototubes were used. The flat-topped voltage plateaus and delay curves obtained indicated 100% efficiency for the counters.

After calibration the crystals were moved to their correct position in the 90° pion channel. Pion identification was based on:

1. Particles passing through the channel as determined by taking differences between the channel open and the channel plugged. Figure 6 shows a 2-in. long brass plug which could be removed or inserted remotely. This defines momentum. Figure 7 shows a typical pair of plug-in plug-out pulse-height distributions. The difference between the two curves is a measure of the pions through the channel.

2. Correct pulse-height amplitude which is a measure of specific ionization.

3. Range of the particles corresponding to the range of pions predicted by wire measurements. Figure 8 shows a range curve obtained for the 40-Mev channel. After allowing for the energy loss in the crystals, the mean pion energy is found to be 40.2 Mev. 50% of the mesons stopped in a thickness of copper equivalent to 2.8 Mev. Analysis of the wire measurements, assuming a constant distribution of mesons over the $\frac{3}{16}$ -in. target, predicts a mean energy of 40.4 Mev and predicts that 50% of the pions should have a spread of 2.5 Mev. The 52-Mev channel yielded similar agreement.

The raw data were corrected for pion decay in flight, multiple-scattering losses, and slit scattering. The largest of these corrections, due to pion decay in flight, is 10%. Since neither the Li⁶ nor the Li⁷ target was 100% pure isotope but contained approximately 8% of the other isotope, a subtraction had to be made to take into account the target contamination. This increased the errors and was particularly unfortunate in

TABLE II. Differential production cross sections for 40- and 52-Mev pions produced in Li⁶ and Li⁷.

Process	Cross section in units of 10^{-32} cm ² Mev ⁻¹ sterad ⁻¹ nucleus ⁻¹
Li ⁷ 40-Mev π^+	19 $\pm 10\%$
Li ⁷ 40-Mev π^-	2.0 $\pm 10\%$
Li ⁷ 52-Mev π^-	0.46 $\pm 10\%$
Li ⁶ 40-Mev π^+	45 $\pm 13\%$
Li ⁶ 40-Mev π^-	0.70 $\pm 29\%$
Li ⁶ 52-Mev π^+	27 $\pm 10\%$
Li ⁶ 52-Mev π^-	0.57 $\pm 14\%$

the case of Li⁷ π^+ at 52 Mev where the correction factor was so large that the result was not reliable.

Table II lists the results together with the errors. The over-all error expressed as a standard deviation includes statistical counting errors, a 5% error in the solid angle, and a 7.5% error in the proton beam.

The striking feature of the above data is the much higher π^+/π^- ratio found for Li⁶ than for Li⁷. Qualitatively this can be explained by Pauli exclusion principle. After pion production, the residual nucleons exist most probably as a mixture of bound and unbound states. The binding energy of the residual nucleons adds to the amount of energy available for pion production and therefore increases the probability of pion production.

TABLE III. Lowest energy reactions leading to pion production.

	Threshold
Li ⁶ + $p \rightarrow$ He ⁴ + 3 p + π^-	167.9 Mev
Li ⁶ + $p \rightarrow$ Li ⁷ + π^+	156.7 Mev
Li ⁷ + $p \rightarrow$ Be ⁷ + p + π^-	161.9 Mev
Li ⁷ + $p \rightarrow$ Li ⁸ + π^+	159.5 Mev

Consider the case of Li⁶. For positive pion production we are left with 3 protons and 4 neutrons while for negative pion production we are left with 5 protons and 2 neutrons. The Pauli principle permits the residual nucleons in the positive pion case to be more tightly bound than in the negative pion case, and hence near threshold for pion production greatly enhances the production of positive pions. For Li⁷, however, the π^- case gives 5 protons and 3 neutrons and the π^+ case gives 3 protons and 5 neutrons. The difference in proton-neutron asymmetry between the two cases is not so large and neither is the binding-energy difference. Therefore, the π^+/π^- difference should be smaller in the Li⁷ case. This is borne out in the threshold values for pion production for the two cases. Table III lists the reactions with the lowest possible threshold energy for the reaction where threshold energy⁶ is given by

$$E = [(m + M_1)^2 - (M_1 + M_2)^2] / 2M_2,$$

where M_0 = total final mass of colliding particles, m = mass of pion, M_2 = mass of target nucleus, and M_1 = mass of proton.

ACKNOWLEDGMENTS

My thanks are due Professor J. B. Platt who supervised this work and to the members of his research group who contributed much help; especially to Professor M. Camac for valuable suggestions, to Mr. B. Johnson for help with the electronics, to Miss J. Kantok for assistance in graphical work, and to Mr. A. England for help in preparing the Li targets.

Thanks are also due Mr. K. Enslin who designed the electronics for the beam energy measurement and to the machine shop crew and the operating crew of the synchrocyclotron.

I am indebted to Professor G. Salzman for helpful discussions.

⁶ R. E. Marshak, *Meson Physics* (McGraw-Hill Book Company, Inc., New York, 1952), p. 73.